Jacek KANIEWSKI, Zbigniew FEDYCZAK

University of Zielona Gora, Institute of Electrical Engineering

Modeling and analysis of dynamic properties of the hybrid transformer with MRC

Abstract. *this paper deals with the modelling and analysis of dynamic properties of the three-phase AC transformer with electromagnetic and electric (hybrid) coupling. The electromagnetic coupling is realized by means of the conventional transformer. The electrical coupling is realized by means of a matrix-reactance chopper (MRC), which is supplied from an auxiliary secondary winding of the transformer. In this paper there are descriptions of the proposed solution, with a presentation of their modeling and analysis of their static and dynamic properties.*

Streszczenie. *Artykuł dotyczy modelowania i analizy stanów dynamicznych trójfazowego transformatora prądu przemiennego ze sprzężeniem elektromagnetycznym i elektrycznym (hybrydowym). Sprzężenie elektromagnetyczne realizowane jest przez konwencjonalny transformator. Sprzężenie elektryczne realizowane jest przez sterownik matrycowo-reaktancyjny zasilany z dodatkowego uzwojenia wtórnego transformatora. W artykule przedstawiono opis działania proponowanego układu z modelowaniem i analizą właściwości statycznych i dynamicznych.* ***(Modelowanie i analiza właściwości dynamicznych transformatora hybrydowego z SMR)***

x

Keywords: -hybrid transformer; matrix-reactance chopper; dynamics; control circuit.
Słowa kluczowe: transformator hybrydowy, sterownik matrycowo-reaktancyjny, dynamika, układ sterowania

Introduction

The dynamic states in AC electric systems, such as faults, fast load changes, switching effects, generate for the consumer undesirable effects like voltage sags, swell and interrupt [1]. In the case of sensitive devices such as computers, transceivers devices, medical systems, erratic supply parameters cause failure or defective devices [2]. In the case of big plants and factories, voltage sags and swells may cause very large financial damage. The application of an AC-AC converter using Pulse Width Modulation (PWM) control strategy to build secondary supply sources (voltage sag and swell compensators and voltage regulators) mitigate the unwanted effects of supply [3]–[5]. The conception of a single–phase new generation distribution transformer is presented in [6], where a conventional transformer works together with a unipolar matrix converter. Circuit with conventional transformer and matrix (MC) or matrix-reactance (MRC) chopper has two couplings (hybrid coupling). Electromagnetic coupling is realized by means of the conventional transformer and electric one realized by means of a matrix converter. From this reason it is called a hybrid transformer (HT). Single phase and three-phase topologies of HT was described in [7]–[11]. Because the hybrid transformers work as voltage sag and swell compensators, voltage regulators and constant-voltage regulators, the dynamic properties, ability to fast response on source voltage changes is very important and desired characteristic. This paper presents three-phase hybrid transformer using buck-boost type matrix-reactance chopper. Presented in this paper there is a description of the proposed solution and an analysis of their static and dynamic properties.

Description of the presented HT. Mine circuit

Schematic diagram of the presented three-phase hybrid transformer (HT) is shown in Fig. 1.

As is visible in Fig. 1 the circuit of the HT contains two main units. The first one is three-phase conventional transformer (TR), with two secondary windings in each phase. The second one is a three-phase buck-boost type matrix-reactance chopper (MRC b-b) [12]. Primary windings are in Y-connections. The main secondary windings (a_1, a_2, a_3) of TR also have Y configurations and, by input filter LC, are connected with the MRC b-b. Secondary phase windings (b_1, b_2, b_3) are connected in series with the required phase output connectors of MRC. Output voltages of HT (u_{L1}, u_{L2}, u_{L3}) are the sum of secondary voltages ($p_b u_{S1}$, $p_b u_{S2}$, $p_b u_{S3}$) and phase output voltages of the MRC. The voltages of the transformer secondary windings a_1, a_2, a_3 and b_1, b_2, b_3 are equal p_a = 4/3 and p_b = 2/3 respectively.

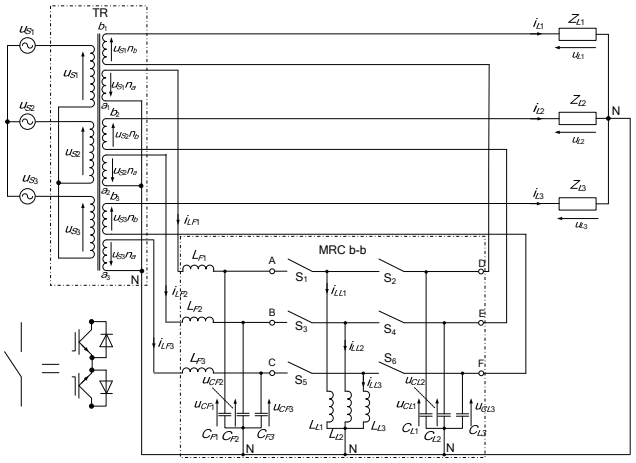

Fig.1. Schematic diagram of the three-phase hybrid transformer with matrix-reactance chopper

Idealized voltage time waveforms illustrating operation of presented HT are shown in Fig. 2.

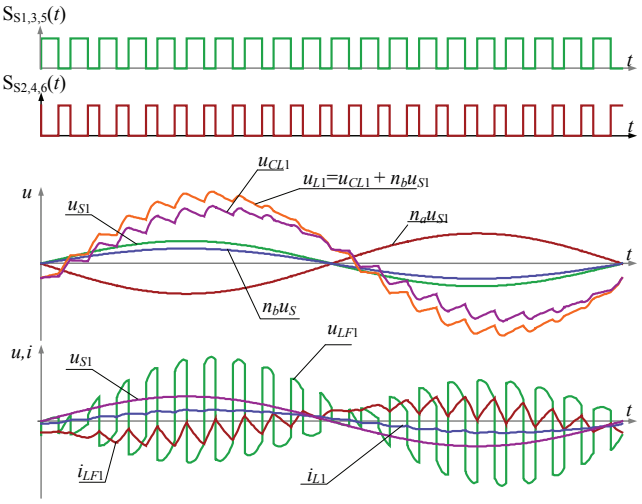

Fig.2. Idealized voltage time waveforms of presented HTfor D=0.6

Exemplary voltage phasors of considered HT are shown in Fig. 3

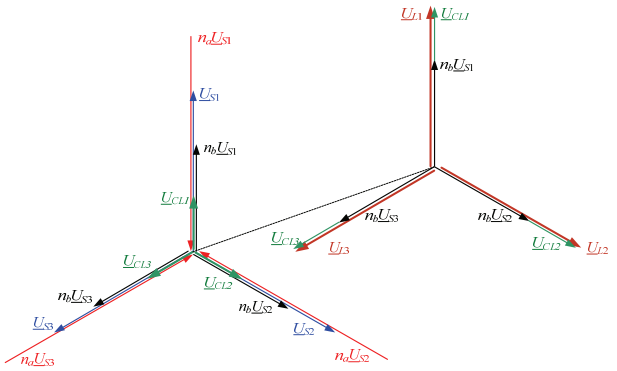

Fig.3. Voltage phasors of presented HT

As is visible in Fig. 2 and Fig. 3, the output voltages of HT is a sum of two voltages (1).

$$\begin{aligned} \underline{U}_{L1} &= n_a \underline{U}_{S1} + \underline{U}_{CL1} \\ \underline{U}_{L2} &= n_a \underline{U}_{S2} + \underline{U}_{CL2} \\ \underline{U}_{L3} &= n_a \underline{U}_{S3} + \underline{U}_{CL3} \end{aligned} \tag{1}$$

where: $n_a\underline{U}_{S1,2,3}$ – secondary voltages of windings $a_{1,2,3}$ of TR, $\underline{U}_{CL1,2,3}$ – output voltages of MRC b-b.

Control circuit of the hybrid transformer

Schematic block diagram of the control circuits is shown in Fig. 4. Main part of circuit contains PI regulator and PWM circuit. The feedback loop include peak detector unit [13].

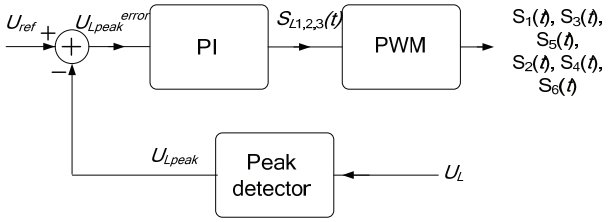

Fig.4. General schematic block diagram of the control circuit

More detailed schematic bloc diagram of the control circuit is shown in Fig. 5.

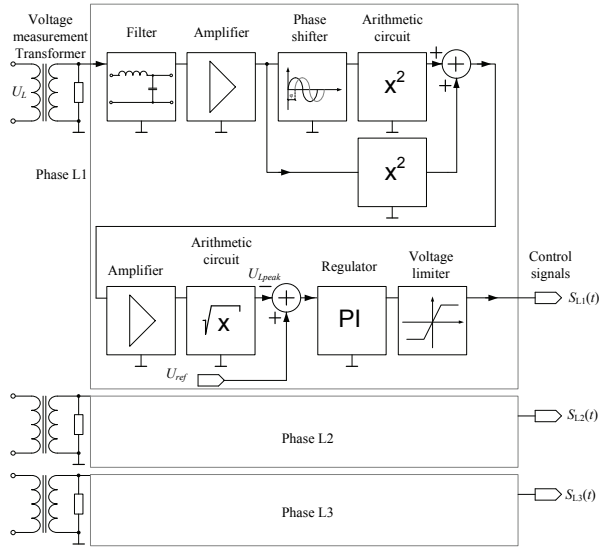

Fig.5. Schematic block diagram of the control circuit

Equation (2) is described the function realized by peak detector unit [13].

$$u_{Lpeak} = \sqrt{\left(U_L \sin(\omega t)\right)^2 + \left(U_L \cos(\omega t)\right)^2} \tag{2}$$

Schematic block diagram of the PWM circuit is shown in Fig. 6.

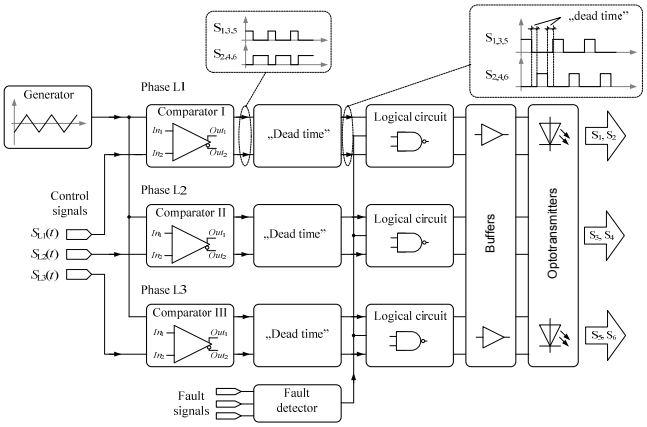

Fig.6. PWM signals circuit

As is visible in Fig. 6 commutation strategy is based on PWM control method with "dead time". Each phase (L1, L2, L3) is controlled independent by control signals $S_{L1}(t)$, $S_{L2}(t)$, $S_{L3}(t)$. Control signals ($S_{L1,L2,L3}(t)$)are a function of the references voltage U_{ref} and load voltage U_L (Fig. 5).

Theoretical analysis. Static properties

Theoretical analysis is based on averaged state space method [15]. Averaged state space equation in general form can be described:

$$\begin{aligned} \dot{\overline{\mathbf{x}}} &= \mathbf{A}(D)\overline{\mathbf{x}} + \mathbf{B}(D)\mathbf{u}_S \\ \overline{\mathbf{y}} &= \mathbf{C}(D)\overline{\mathbf{x}} + \mathbf{D}(D)\mathbf{u}_S \end{aligned} \tag{3}$$

where: $\overline{\mathbf{x}}$ - vector of the averaged variables, $\mathbf{A}(D)$ – averaged state matrix, $\mathbf{B}(D)$ – averaged input matrix, $\mathbf{C}(D)$ – averaged output matrix, $\mathbf{D}(D)$ – averaged input-output matrix.

According to (3) averaged state space equation of the considered circuit of HT (Fig. 1) in matrix form can be described as:

(4)

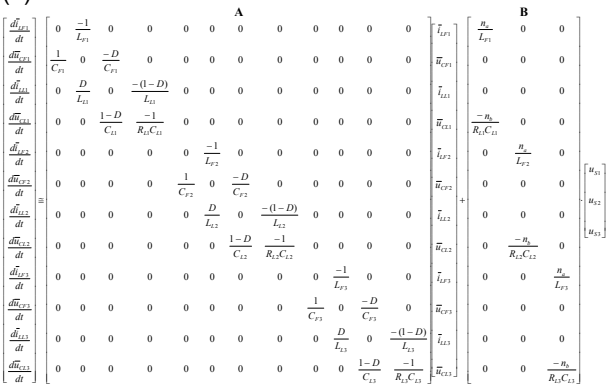

Take into account (4) is constructed averaged circuit model of HT (Fig. 7).

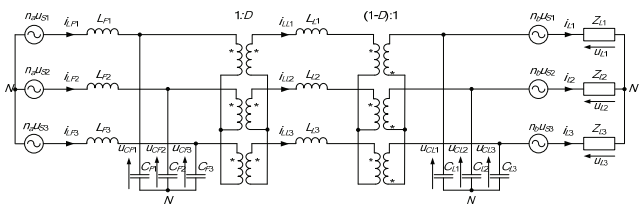

Fig.7. Three-phase averaged circuit model of HT

Assuming symmetrical and balanced circuit of presented HT and using d-q transformation method (5), we can describe it as single phase circuit [9], [10], [15] (Fig. 8).

(5) $$\mathbf{x}_{d-q} = \mathbf{K}\mathbf{x}_{abc}$$

where:

$$\mathbf{K} = \sqrt{\frac{2}{3}}\begin{bmatrix} \cos(\omega t) & \cos(\omega t - \frac{2\pi}{3}) & \cos(\omega t + \frac{2\pi}{3}) \\ \sin(\omega t) & \sin(\omega t - \frac{2\pi}{3}) & \sin(\omega t + \frac{2\pi}{3}) \\ \frac{1}{\sqrt{2}} & \frac{1}{\sqrt{2}} & \frac{1}{\sqrt{2}} \end{bmatrix}$$

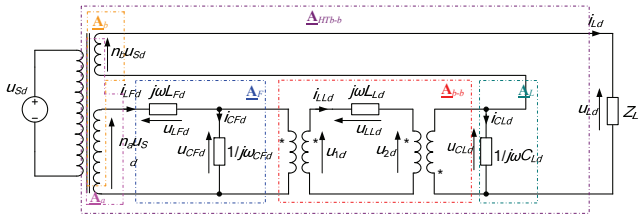

Fig.8. Equivalent schematic diagram of HT

Averaged circuit model (Fig. 8) is divided into four terminal networks. Applying the four-terminal description method and procedure described by figure 9 we obtain equation (6).

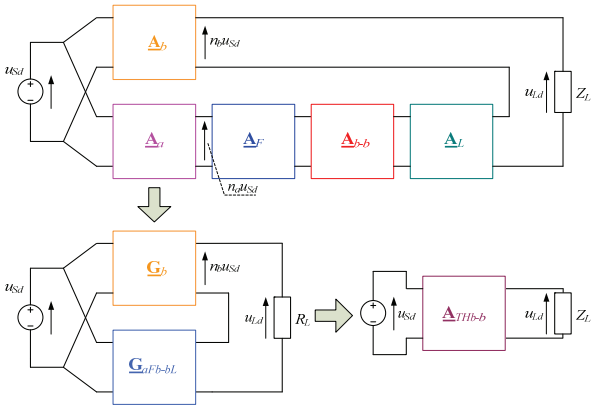

Fig.9. Equivalent schematic diagram of HT

(6) $$\begin{bmatrix} \underline{U}_S \\ \underline{I}_S \end{bmatrix} = \underline{\mathbf{A}}_{THb-b}\begin{bmatrix} \underline{U}_L \\ \underline{I}_L \end{bmatrix} = \begin{bmatrix} \underline{A}_{THb-b11} & \underline{A}_{THb-b12} \\ \underline{A}_{THb-b21} & \underline{A}_{THb-b22} \end{bmatrix}\begin{bmatrix} \underline{U}_L \\ \underline{I}_L \end{bmatrix} = \frac{1}{\underline{G}_{THb-b21}}\begin{bmatrix} 1 & -\underline{G}_{THb-b22} \\ \underline{G}_{THb-b11} & -\det\underline{\mathbf{G}}_{THb-b} \end{bmatrix}\begin{bmatrix} \underline{U}_S \\ \underline{I}_L \end{bmatrix},$$

(7) $$\underline{\mathbf{G}}_{THb-b} = \underline{\mathbf{G}}_b + \underline{\mathbf{G}}_{aFb-bL}.$$

where **G** – matrix of hybrid parameters G-type.

In accordance with four terminal theories, we obtain:

(8) $$\underline{H}_U = \frac{\underline{U}_L}{\underline{U}_S} = \frac{1}{\underline{A}_{HT11} + \underline{A}_{HT12}/Z_L},$$

(9) $$\arg\underline{H}_U = \arg\left(\frac{1}{\underline{A}_{HT11} + \underline{A}_{HT12}/Z_L}\right),$$

(10) $$\lambda_S = \frac{P_S}{S_S} = \cos\left[\arg\left(\frac{\underline{A}_{HT11}R_L + \underline{A}_{HT12}}{\underline{A}_{HT21}R_L + \underline{A}_{HT22}}\right)\right].$$

Static characteristics of presented HT are shown in Figs. 15 - 17 in the section "Simulation and experimental test results".

Dynamic properties

It is assumed that all variables have two components: a running constant component [15] (the averaged value in the switching period T_S), which is marked by upper case letter, and perturbation marked by lower case letter, straddled by the symbol "^".

(11) $$i_{LF} = I_{LF} + \hat{i}_{LF}, u_{CF} = U_{CF} + \hat{u}_{CF}, i_{LL} = I_{LL} + \hat{i}_{LL}$$
$$u_{CL} = U_{CL} + \hat{u}_{CL}, d = D + \hat{d}$$

(12) $$\frac{d}{dt}(\mathbf{X} + \hat{\mathbf{x}}) \approx \mathbf{A}\hat{\mathbf{x}} + \mathbf{B}\hat{\mathbf{u}} + [(\mathbf{A}_1 - \mathbf{A}_2)\mathbf{X} + (\mathbf{B}_1 - \mathbf{B}_2)\mathbf{U}]\hat{d}$$

where $\mathbf{A}_1 = \mathbf{A}(D)$ for $D = 0$, $\mathbf{A}_2 = \mathbf{A}(D)$ for $D = 1$. According to (12), the Laplace transform for small signal state-space equation is expressed as (13) and (14):

(13) $$s\hat{\mathbf{x}}(s) = \mathbf{A}\hat{\mathbf{x}}(s) + \mathbf{B}\hat{\mathbf{u}}(s) + [(\mathbf{A}_1 - \mathbf{A}_2)\mathbf{X} + (\mathbf{B}_1 - \mathbf{B}_2)\mathbf{U}]\hat{d}(s),$$

(14) $$\hat{u}_L(s) = \mathbf{C}\hat{\mathbf{x}}(s) + \mathbf{D}\hat{\mathbf{u}}(s).$$

Solving equation (13) and (14) we obtain (15) and (16).

(15) $$\hat{\mathbf{x}}(s) = (s\mathbf{I} - \mathbf{A})^{-1}\{\mathbf{B}\hat{\mathbf{u}}(s) + [(\mathbf{A}_1 - \mathbf{A}_2)\mathbf{X} + (\mathbf{B}_1 - \mathbf{B}_2)\mathbf{U}]\hat{d}(s)\} = \mathbf{G}_{\hat{\mathbf{x}},\hat{\mathbf{u}}}(s)\mathbf{u}(s) + \mathbf{G}_{\hat{\mathbf{x}},\hat{d}}(s)\hat{d}(s)$$

(16) $$\hat{u}_L(s) = [\mathbf{C}\mathbf{G}_{\hat{\mathbf{x}},\hat{\mathbf{u}}}(s) + \mathbf{D}]\hat{\mathbf{u}}(s) + [\mathbf{C}\mathbf{G}_{\hat{\mathbf{x}},\hat{d}}(s)]\hat{d}(s) = \mathbf{G}_{\hat{u}_L,\hat{\mathbf{u}}}(s)\hat{\mathbf{u}}(s) + \mathbf{G}_{\hat{u}_L,\hat{d}}(s)\hat{d}(s),$$

where:

(17) $$\mathbf{G}_{\hat{\mathbf{x}},\hat{\mathbf{u}}} = \frac{\hat{\mathbf{x}}(s)}{\hat{\mathbf{u}}(s)},$$ (18) $$\mathbf{G}_{\hat{\mathbf{x}},\hat{d}} = \frac{\hat{\mathbf{x}}(s)}{\hat{d}(s)}$$

(19) $$\mathbf{G}_{\hat{u}_L,\hat{\mathbf{u}}} = \frac{\hat{u}_L(s)}{\hat{\mathbf{u}}(s)},$$ (20) $$\mathbf{G}_{\hat{u}_L,\hat{d}} = \frac{\hat{u}_L(s)}{\hat{d}(s)}$$

The calculation and simulation test results of the transient states of the considered HT are shown in Fig. 17 in the section "Simulation and experimental test results".

Stability

Equivalent block diagram of considered hybrid transformer is shown in Fig. 10.

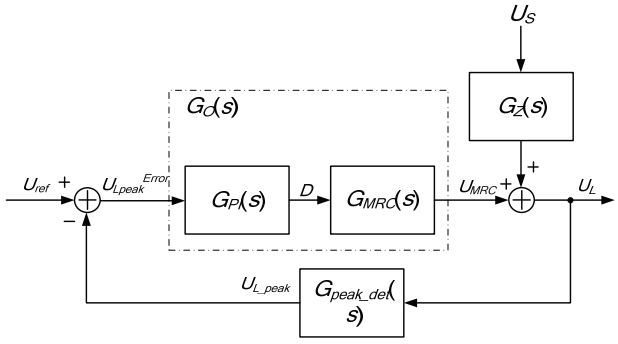

Fig.10. Equivalent block diagram of presented HT

Transmittance of the MRC can be described as:

(21) $$G_{MRC}(s) = G_D(s) \cdot G_F(s)$$

where G_D – linearized characteristic of MRC (22), G_F – input filter transmittance (23).

(22) $$G_D(s) = \frac{\Delta U_{MRC}}{\Delta D} = k_{MRC},$$

(23) $$G_F(s) = \frac{1}{s^2 L_F C_F + s R_L C_F + 1}$$

Transmittance of PI regulator is described as (24).

(24) $$G_{PI}(s) = \frac{\Delta D}{\Delta U_{Lpeak}^{Error}} = K_P\left(1 + \frac{1}{T_I s}\right),$$

(25) $$G_O(s) = \frac{\Delta U_{MRC}}{\Delta U_{Lpeak}^{Error}} = G_{PI}(s) \cdot G_{MRC}(s).$$

Take into account (25) and assuming transmittance of peak detector equal 1 (G_{peak_def}(s) = 1), the main transmittance of circuit shown in figure 10 can be described as (26).

(26) $$G_{HT}(s) = \frac{G_O}{1 + G_O},$$

(27) $$G_{error}(s) = \frac{1}{1 + G_O},$$

(28) $$G_Z(s) = G_{nb}(s) + G_{na}(s) \cdot G_{MRC}(s) = n_b + n_a G_{MRC}(s).$$

Take into account (28) distortion transmittance can be described as (29).

(29) $$G_{dist}(s) = \frac{G_Z(s)}{1 + G_O(s)}.$$

Time waveforms of step response (26) and control error (27) are shown in Figs. 18 and 19 respectively.

Simulation and experimental test results

The parameters of the circuit shown in Fig 1, which has been investigated, are collected in the appendix in table I. The presented results have been obtained for matching conditions described by (30)

(30) $$\sqrt{\frac{L}{C}} \approx \sqrt{\frac{L_F}{C_F}} \approx \sqrt{\frac{L_L}{C_L}} \approx |Z_L|.$$

Experimental voltage time waveforms during step up and step down of duty factor value D are shown in Fig 11 and Fig. 12 respectively.

As is visible in Figs 11 and 12, response of the load voltage during step up/down of D is very fast (≈ 2ms). Experimental voltage time waveforms during source voltage u_{S2} swell are shown in Fig 13.

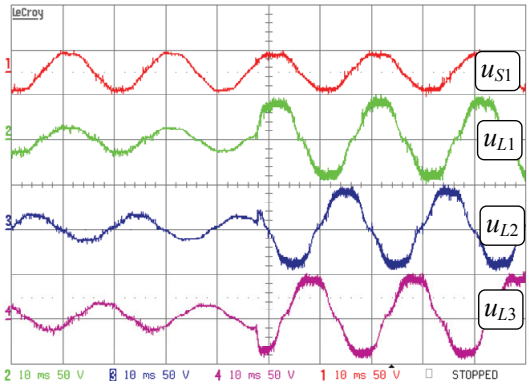

Fig.11. Experimental voltage time waveforms for step up duty factor from D=0.1 to D = 0.6

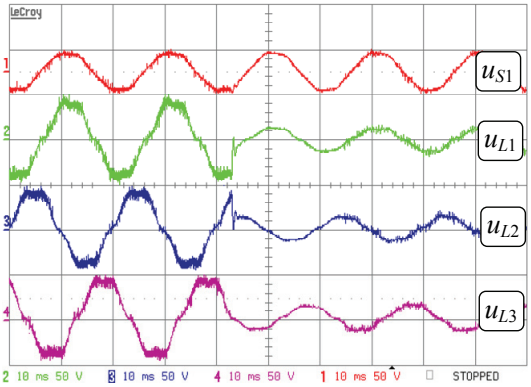

Fig.12. Experimental voltage time waveforms for step down duty factor from D=0.6 to D = 0.1

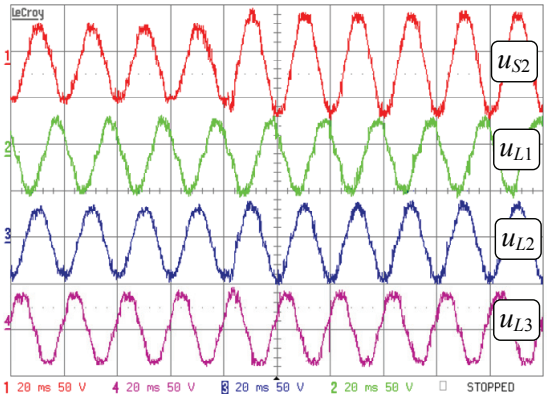

Fig.13. Experimental voltage time waveforms during 40% source over voltage

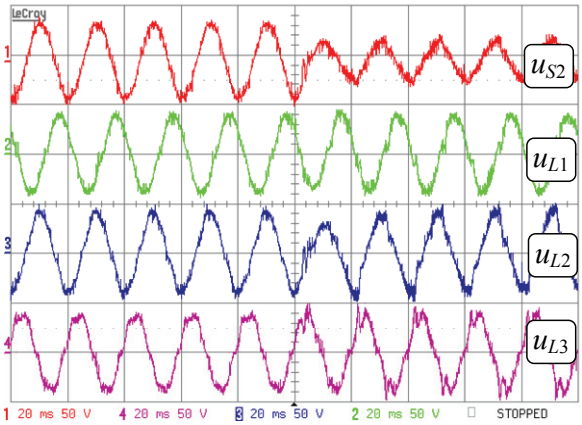

Fig.14. Experimental voltage time waveforms during more then 50% source voltage sag

As is visible in Fig. 13 during 40% voltage swell the output voltages u_L has constant value all the time. Experimental voltage time waveforms during over 50% source voltage u_{S2} sag are shown in Fig 13. Static characteristic of voltage magnitude, phase and input power factor are shown in Figs. 15–17. In the circuit with presented HT, the range of change of output voltage is from $0.66u_S$ to more then $3u_S$ (Fig. 15). A phase shift between source and load voltage is caused by passive elements in MRC structure.

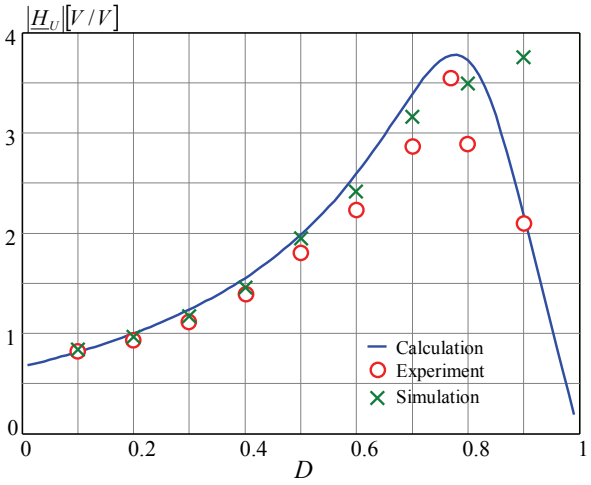

Fig.15. Magnitude of voltage transmittance as a function of the pulse duty factor *D*

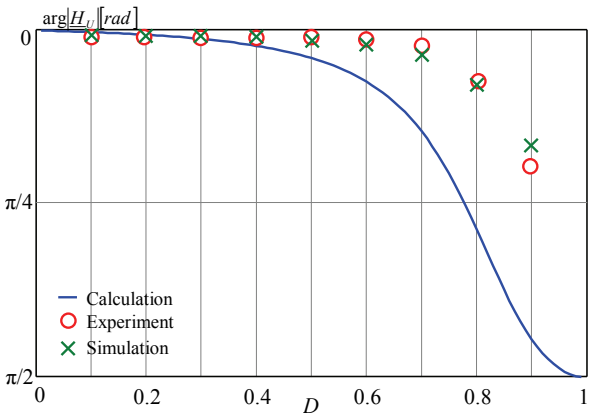

Fig.16. Phase of voltage transmitance as a function of the pulse duty factor *D*

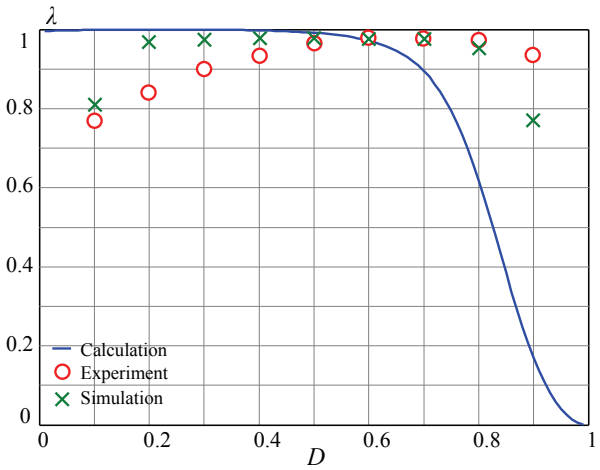

Fig.17. Input power factor depending on duty factor *D*

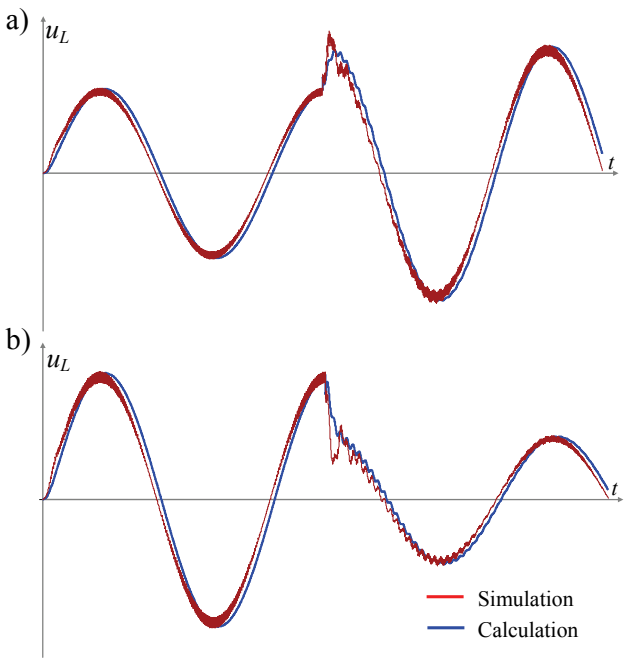

Fig.18. Load voltage during a) 50% step up of source voltage, b) 50% step down of source voltage

As is visible in Figs. 13, 14 and 18, the transient state during source voltage step up/dawn is about 10 ms. Time waveforms of control error and step response of presented HT are shown in Figs 19 and 20 respectively.

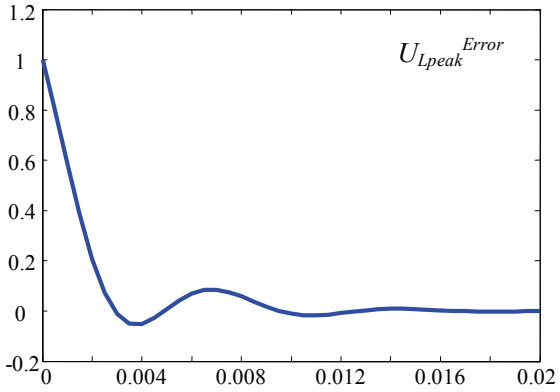

Fig.18. Control error

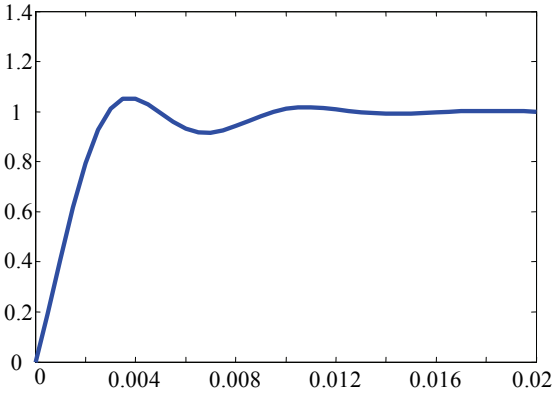

Fig.19. Step response

Conclusions

In this paper the results of modeling an analysis of a three–phase hybrid transformer using buck-boost type matrix-reactance chopper has been presented. Modeling of HT is based on averaging method and four–terminal description method. Generally the results of the simulation investigation confirm the results of theoretical study. The range of change of output voltage gives the possibility of using proposed HT for compensation of 50% sags and over 50% swells of source voltage. Further research will be focused on detailed analysis of non-balanced circuit analysis.

Appendix

Table 1. Circuit parameters

Parameter	name	value	unit
p_a	voltage ratio	4/3	-
p_b	voltage ratio	2/3	-
L_F / L_L	MRC inductance	1	mH
C_F / C_L	MRC capacitance	10	μF
Z_L	Load impedance	60	Ω
f_s	switching frequency	5	kHz
u_S	supply voltage	50	V

REFERENCES

[1] J. Milanowić, I. Hiskansen: "Effect of load dynamics on power system damping," *IEEE Trans. on Power System* Vol. 10 No. 2, pp. 1022 -1028 May 1995

[2] Z. Djokic, J. Desment, G. Vanalme, J. Milanovic, K. Stockman: "Sensitivity of personal computer to voltage sags and short interruptions," *IEEE Trans. on Power Delivery*, vol. 20, No.1, pp. 375 - 383 Jan. 2005.

[3] E. Aeloiza, P. Prased, P. Enjeti, L. Moran, O. Montero-Hernandez, S. Kim.: Analysis and design of new voltage sag compensator for critical loads in electric power dystrybution system. *IEEE Trans. on Ind. Applications*, vol. 39 No.4, pp.1143 - 1150 July / Aug. 2003

[4] O. Montero-Hernandez, P. Enjeti: "Application of a boost ac-ac converter to compensate for voltage sags in electric power distribution system," in Proc. 2000 IEEE *31TH Power Engineering Society Transmission and Distribution* Conf. pp. 470 – 475.

[5] S. Subramanian, M. K. Mishra, "Interphase AC-AC topology vor sag supporter", *IEEE Tran. on Power Elec*, vol. 25, No. 2, Feb. 2010

[6] E. Aeloiza, P. Enjeti, L. Moran, I. Pite: Next generation distribution transformer: to address power quality for critical loads .*PESC'03 IEEE* vol. 3 pp.1266 – 1271 June 2003.

[7] J. Kaniewski: "Single phase hybrid transformer using matrix converter" Wiadomości Elektrotech. 03.2006, pp: 46-48. (In Polish)

[8] Z. Fedyczak, J. Kaniewski: "Single phase hybrid transformer using bipolar matrix – reactance chopper," *Przegląd Elektrotechniczny* 07-08.2006, pp: 80-85. (In Polish)

[9] Fedyczak Z, Kaniewski J., "Modeling and analysis of three-phase hybrid transformer using matrix converter", *Compatibility in Power Electronics - CPE 2007,* 5th International Conference-Workshop. Gdańsk, Polska, 2007, Gdynia, 2007

[10] Kaniewski J, Fedyczak Z., "Modelling and analysis of three-phase hybrid transformer using matrix-reactance chopper", *Przegląd Elektrotechniczny*, 2009, nr 2, s. 100-105

[11] Kaniewski J., Fedyczak Z., Klytta M., Łukiewski M., Szcześniak P.,"Implementation of a three-phase hybrid transformer using a matrix chopper", *13th European Conference on Power Electronics and Applications*, EPE 2009. Barcelona, Hiszpania, 2009

[12] Z. Fedyczak: PWM AC voltage transforming circuits,. *University of Zielona Góra Press*, Zielona Góra 2003. (In Polish)

[13] Chu H. Y., Jou H. L., C Huang. L.: Transient response of a peak voltage detector for sinusoidal signals, *IEEE Trans. on Ind. Electronics*, vol. 39, No. 1 February 1992

[14] C. T. Rim, D. Y. Hu, G. H. Cho: "Transformers as Equivalent Circuits for Switches: General Proofs and D-Q Transformation – Based Analyses," *IEEE Trans on Ind Apl*. vol.26 No. 4 July/Aug 1990

[15] Middlebrock R. D., Ćuk S.: "General unified approach to modeling switching converter power stages". Rec. *IEEE PESC*,76, pp. 18 – 34, 1976

***Authors**: mgr inż. Jacek Kaniewski, dr hab. inż. Zbigniew Fedyczak prof. UZ, University of Zielona Góra, Instytut of Electrical Engineering, ul.Podgórna 50, 65-246 Zielona Góra, Poland, E-mail: J.Kaniewski@iee.uz.zgora.pl, Z.Fedyczak@iee.uz.zgora.pl*